ChemComm

COMMUNICATION

View Article Online
View Journal | View Issue

Cite this: *Chem. Commun.*, 2015, 51, 7309

Received 26th January 2015,
Accepted 22nd March 2015

DOI: 10.1039/c5cc00751h

www.rsc.org/chemcomm

Thermally-activated recombination in one component of $(CH_3NH_3)PbI_3/TiO_2$ observed by photocurrent spectroscopy†

Patrick Cottingham,[a] David C. Wallace,[a] Ke Hu,[b] Gerald Meyer[b] and Tyrel M. McQueen*[acd]

Photocurrent measurements on devices containing perovskite $(CH_3NH_3)PbI_3$ show two distinct spectral responses when deposited in a mesoporous oxide matrix, compared with one response for planar perovskite alone. With a TiO_2 matrix, the shorter wavelength response has an inverted temperature response with increasing performance on cooling.

Organometallic halide perovskites have been the subject of intense research in recent years. Interest in these materials stems in part from their ability to function as efficient light absorbers and electron- and hole-transport materials in photovoltaic (PV) devices. These materials are especially attractive for PV applications because of their earth-abundant components and the wide variety of low-energy synthetic techniques[1–4] by which they can be produced. Early studies of PV devices containing organometallic halide perovskites used perovskite $(CH_3NH_3)PbI_3$ deposited into a mesoporous TiO_2 matrix.[5–7] Later studies demonstrated that efficient devices could be constructed using $(CH_3NH_3)PbI_3$ and larger-bandgap oxides such as Al_2O_3 and ZrO_2 in which the energy of the conduction band minimum is too high for electron injection from $(CH_3NH_3)PbI_3$ to occur.[8–11] Perovskite PV cells not containing any oxide matrix ('planar' devices) have also produced high efficiencies.[1,2,9,12]

It has been suggested that in addition to providing a driving force for charge separation at the $(CH_3NH_3)PbI_3/TiO_2$ interface, TiO_2 enhances the performance of devices by acting as an electron-transport material.[13] However, devices with $(CH_3NH_3)PbI_3$ deposited in highly-insulating Al_2O_3, where the conduction band minimum of the oxide is well above that of perovskite, achieve similar or better performance than devices on TiO_2.[8] Given the performance of Al_2O_3-containing devices, the role of the oxide matrix in charge separation remains unclear.

A recent study of the structure of $(CH_3NH_3)PbI_3$ in a TiO_2 matrix shows that the matrix has a profound effect on the structure of perovskite.[14] PDF (pair distribution function) analysis of X-ray total scattering data suggests that when $(CH_3NH_3)PbI_3$ is deposited into mesoporous TiO_2 it forms two components with the same crystal structure: a relatively disordered component consisting of ~1.4 nm diameter nanocrystals which are confined by pores of the matrix and one with much longer-range coherence. More recent work suggests that the catalytic action of water may be essential for the formation of the perovskite phase.[15]

In order to explore the mechanisms of charge separation in planar devices *versus* devices based on TiO_2 or highly-insulating oxides, we report temperature-dependent photocurrent measurements on a range of devices. The planar perovskite (Fig. 1a) and perovskite on mesoporous TiO_2 or ZrO_2 (Fig. 1b) devices were prepared following published procedures.[6] X-ray diffraction was used to check film purity (see Fig. S1, ESI†). Briefly, 40.3 weight% perovskite precursor solution was prepared with an equimolar ratio of CH_3NH_3I and PbI_2 in γ-butyrolactone and spin-coated onto an FTO (fluorine-doped tin oxide) substrate or onto mesoporous TiO_2 or ZrO_2 on an FTO substrate. (see ESI† for details). The substrates were mechanically compressed against a nickel foil electrode using a spring-loaded clamp.

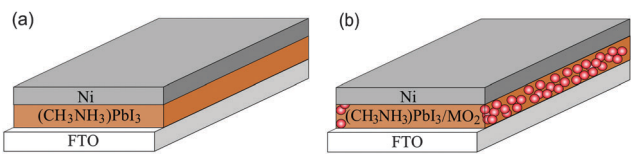

Fig. 1 Schematic illustration of two devices containing $(CH_3NH_3)PbI_3$. All devices contain an absorber layer compressed between one FTO electrode and one nickel electrode. The device in (a) contains a planar $(CH_3NH_3)PbI_3$ absorber layer. The device in (b) contains $(CH_3NH_3)PbI_3$ embedded in a mesoporous MO_2 matrix, where M is Ti or Zr.

[a] *Department of Chemistry, Johns Hopkins University, 3400 N. Charles St., Baltimore 21218, USA. E-mail: mcqueen@jhu.edu*
[b] *Department of Chemistry, University of North Carolina at Chapel Hill, 123 South Rd., Chapel Hill, NC 27599, USA*
[c] *Department of Physics and Astronomy, Johns Hopkins University, 3400 N. Charles St., Baltimore 21218, USA*
[d] *Department of Materials Science and Engineering, Johns Hopkins University, 3400 N. Charles St., Baltimore 21218, USA*

† Electronic supplementary information (ESI) available. See DOI: 10.1039/c5cc00751h

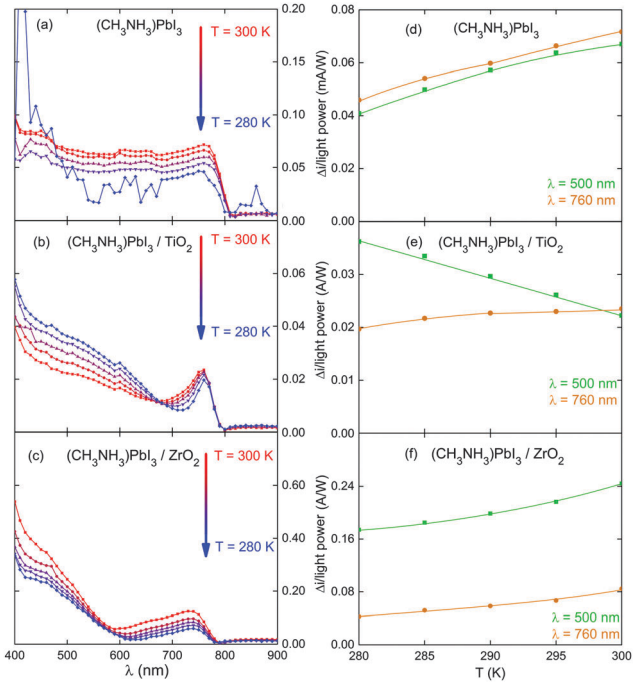

Fig. 2 (a), (b), and (c) Respectively show the photocurrent of devices containing planar $(CH_3NH_3)PbI_3$, $(CH_3NH_3)PbI_3$ in TiO_2, and $(CH_3NH_3)PbI_3$ in ZrO_2 as a function of temperature. (d), (e), and (f) Show the photocurrent of those devices at λ = 500 nm, and λ = 760 nm as a function of temperature. All lines are guides to the eye. Noise at T = 280 K is due to failure of the light bulb.

Photocurrent measurements were conducted by mounting the samples on a bespoke probe and illuminating the samples using a monochromated lamp. All data is normalized per Watt of incident light (see ESI† for details).

Fig. 2a shows the photocurrent of the device containing planar $(CH_3NH_3)PbI_3$. The photocurrent is approximately constant with wavelength from λ = 400 nm until the photocurrent onset at λ = 800 nm. This spectral shape is commonly associated with the photoconductivity of a direct-bandgap semiconductor. In devices of this kind, containing neither a strong interfacial electric field nor a dedicated electron- or hole-transport layer, charge separation may occur by diffusion.[16] As the temperature of the sample is decreased, the photocurrent decreases at all wavelengths above the photocurrent edge by an approximately constant factor.

Fig. 2b shows the photocurrent of a device with mesoporous TiO_2. The photocurrent spectrum for this device contains two distinct responses. The first response is centered at shorter wavelengths and shows a gradual decrease in intensity on scanning to longer wavelengths. The second response has a peak-like shape and is centered at around λ = 760 nm. This kind of distinct upturn near the band-edge has been previously observed in devices containing $(CH_3NH_3)PbI_3$ and oxide when the data is reported in terms of external quantum efficiency.[2,17,18] The photocurrent of $(CH_3NH_3)PbI_3$ in mesoporous ZrO_2 (Fig. 2c) shows two similarly shaped responses.

A plausible explanation for the appearance of two responses in the photocurrent when $(CH_3NH_3)PbI_3$ is deposited on a mesoporous matrix is the formation of two components as observed by Choi *et al.*;[14] this is also consistent with our observation that planar $(CH_3NH_3)PbI_3$ devices with a compact, but not mesoporous, TiO_2 layer also only show a single response (Fig. S2, ESI†). The peak-like shape of the longer-wavelength response is reminiscent of a quantum dot, suggesting that it derives from the short-range ordered component. However, quantum confinement effects blue-shift the absorption of nanocrystals, suggesting that the photocurrent at shorter wavelengths derives from the short-range ordered component. If the shorter-wavelength response does correspond to the short-range ordered component, the Brus equation[19] for the energy of transitions in a semiconductor cluster (eqn (1))

$$\Delta E(r) = E_{\mathrm{gap}} + \frac{h^2}{8r^2}\left(\frac{1}{m_{\mathrm{e}}^*} + \frac{1}{m_{\mathrm{h}}^*}\right) \quad (1)$$

can be used to calculate the effective mass of a free carrier in this component by assuming that the electron and hole effective masses, m_{e}^* and m_{h}^*, are equal. $\Delta E(r)$ is the energy of the transition in the cluster, E_{gap} is the bandgap of the bulk semiconductor, r is the radius of a cluster, and h is the Planck constant. The effective mass calculated using this equation is $m^* = 15m_0$, which differs substantially from the values of $m_{\mathrm{e}}^* = 0.23m_0$ and $m_{\mathrm{h}}^* = 0.29m_0$ determined from density functional theory (DFT) calculations.[20] This discrepancy suggests that the difference in the photocurrent edge between the two components derives from differences in structure, composition, or disorder or from space-charge effects rather than quantum confinement.

As it is not possible to definitively assign the two features in the photocurrent spectrum to either the short-range ordered or the medium-range ordered component of $(CH_3NH_3)PbI_3$, they will be referred to below as component 1 (giving rise to the feature at shorter wavelengths) and component 2 (giving rise to the feature centered at λ = 760 nm).

Plotting the photocurrent at λ = 500 nm and λ = 760 nm as a function of temperature shows profound differences between different devices. For planar $(CH_3NH_3)PbI_3$ (Fig. 2d), the responses at both wavelengths vary almost linearly with temperature and have approximately the same positive slope. For $(CH_3NH_3)PbI_3$ in TiO_2, however, the response at λ = 500 nm decreases with increasing temperature while the response at λ = 760 nm increases with increasing temperature (Fig. 2e). For $(CH_3NH_3)PbI_3$ in ZrO_2, the two response at both wavelengths both increase with increasing temperature (Fig. 2f).

The short-wavelength photocurrent efficiency decreases with increasing temperature for the TiO_2-containing devices and increases for all other samples; this implies that TiO_2 is responsible for this behaviour.

The changes in photocurrent at λ = 500 nm for the TiO_2-containing devices can be described well by an expression for thermally activated recombination containing a constant term which represents the photocurrent in the absence of recombination and an Arrhenius-type term which accounts for recombination (eqn (2)). Here Δi is the measured photocurrent normalized for the incident light intensity, E_{a} is the energy barrier for recombination, C is a constant which represents the photocurrent in the absence of recombination, and A is a free scaling parameter. The sign of A is

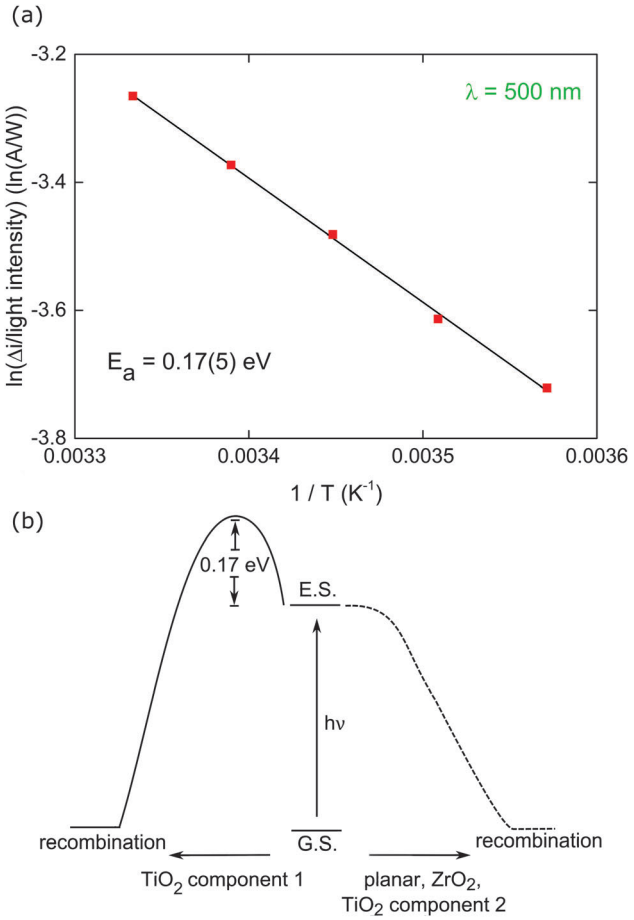

Fig. 3 (a) Shows a fit to the change in photocurrent as a function of temperature for the device containing $(CH_3NH_3)PbI_3$ in TiO_2 at λ = 500 nm. (b) Shows a model of charge recombination in component 1 of $(CH_3NH_3)PbI_3$ in TiO_2, compared with planar $(CH_3NH_3)PbI_3$, $(CH_3NH_3)PbI_3$ in ZrO_2, and component 2 of $(CH_3NH_3)PbI_3$ in TiO_2.

opposite to that of Δi and C because the Arrhenius term represents recombination which reduces the overall photocurrent.

$$\Delta i = C + Ae^{\frac{-E_a}{k_B T}} \quad (2)$$

If the value of C = 0.06(1) A/W determined from fitting is subtracted from Δi, the Arrhenius term can be isolated and shown in a typical $\ln(k)$ *vs.* $1/T$ -type plot (Fig. 3a). The energy barrier determined from the fit is E_a = 0.17(5) eV. The results of the fit can be used to construct a model of charge recombination for the three devices (Fig. 3b). For all of the devices, free charge carriers are generated when the absorption of a photon generates an electron–hole pair. For planar $(CH_3NH_3)PbI_3$, component 2 of $(CH_3NH_3)PbI_3$ in TiO_2, and both components of $(CH_3NH_3)PbI_3$ in ZrO_2, recombination proceeds through a pathway in which thermal activation is not the rate-limiting step. In contrast, for component 1 of $(CH_3NH_3)PbI_3$ in TiO_2, recombination occurs with an effective energy barrier of E_a = 0.17(5) eV.

The absence of thermally-activated recombination in component 2 of $(CH_3NH_3)PbI_3$ in TiO_2 suggests that charge collection from this component proceeds through a pathway not involving TiO_2, perhaps involving percolation through a network of nano-scale domains. It is plausible for such networks to exist given Choi *et al.*'s observation[14] that ~70% of $(CH_3NH_3)PbI_3$ on TiO_2 consists of the short-range ordered component.

The thermally-activated recombination of carriers from component 1 of $(CH_3NH_3)PbI_3$ in TiO_2 likely consists of a combination of back-electron transfer and/or recombination related to transport through TiO_2. Experimentally determined values for the offset between the conduction band minima of $(CH_3NH_3)PbI_3$ and TiO_2 range from 0.07 eV[7] to 0.4 eV.[21] DFT including spin–orbit coupling has been used to calculate an offset of 0.2 eV.[22] With an energy offset in this range electron transfer from TiO_2 to $(CH_3NH_3)PbI_3$ is possible. This is in contrast to ZrO_2 where the conduction band minimum is more than 1 eV above that of TiO_2[23] and electron transfer to the oxide is unlikely. Studies of transport in TiO_2-based dye-sensitized solar cells (DSSCs) have also found activation energies for electron mobility of E_a = 0.15 eV.[24] The thermal activation of recombination may involve transport to recombination sites in TiO_2 or to an interface where recombination or back-electron transfer occurs.

It is unclear from the data above why charge injection to TiO_2 does not occur from component 2. One explanation is that this component is physically separated from TiO_2, likely by component 1. Alternately, it is possible that the conduction band minimum of component 2 is below that of TiO_2 and carriers diffuse away from the $(CH_3NH_3)PbI_3/TiO_2$ interface before hot-carrier or thermally-activated injection can occur.

One aspect of the photocurrent data which is not fully explained by the model in Fig. 3b is the substantially larger photocurrent at all wavelengths of the device containing $(CH_3NH_3)PbI_3$ on ZrO_2. The difference may result from differences in sample thickness. Scanning electron microscopy (SEM) imaging shown in Fig. 4 indicates that the TiO_2-containing samples were ~2.5 times thicker than ZrO_2-containing samples. This difference is approximately the same as the difference in photocurrent between the samples at longer wavelengths where injection into TiO_2 is not a factor. Similar decreases in incident photon conversion efficiency (IPCE) have been observed with increasing $(CH_3NH_3)PbI_3/TiO_2$ layer thickness for complete PV cells and has been attributed to increased recombination.[25]

The observation of two distinct responses in the photocurrent spectra of devices containing $(CH_3NH_3)PbI_3$ on an oxide matrix, compared to one response for planar $(CH_3NH_3)PbI_3$, supports previous crystallographic observations of two distinct components in $(CH_3NH_3)PbI_3$ on TiO_2. The inverted temperature dependence of the photocurrent from one component of $(CH_3NH_3)PbI_3$ in TiO_2 indicates that thermally activated recombination occurs when charge injection and transport occur through TiO_2. The other component of $(CH_3NH_3)PbI_3$ in TiO_2 appears to separate and transport charge through a mechanism not involving TiO_2. Fitting the activation energy of recombination with an Arrhenius term gives an energy barrier for recombination of E_a = 0.17(5) eV.

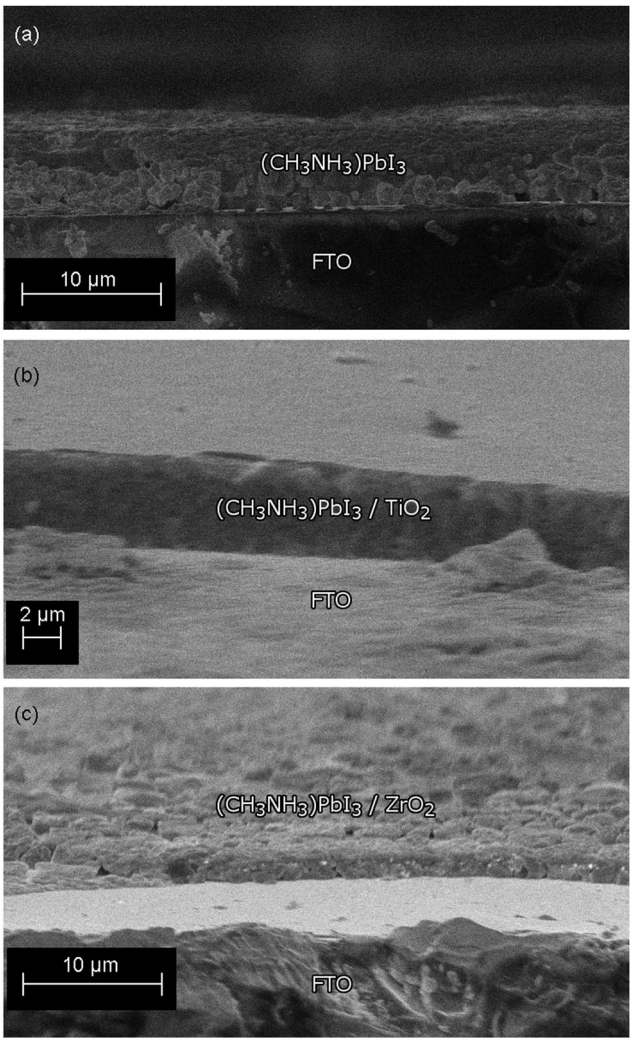

Fig. 4 Scanning electron microscope (SEM) images of (a) planar $(CH_3NH_3)PbI_3$, (b) $(CH_3NH_3)PbI_3$ in TiO_2, and (c) $(CH_3NH_3)PbI_3$ in ZrO_2.

Work supported by the American Chemical Society Division of Inorganic Chemistry Exxon-Mobil Solid State Faculty Fellowship and the National Science Foundation (NSF) Division of Materials Research (DMR) CAREER grant #1253562.

Notes and references

1 M. H. Kumar, N. Yantara, S. Dharani, M. Grätzel, S. Mhaisalkar, P. P. Boix and N. Mathews, *Chem. Commun.*, 2013, **49**, 11089.
2 J. You, Z. Hong, Y. Yang, Q. Chen, M. Cai, T.-B. Song, C.-C. Chen, S. Lu, Y. Liu, H. Zhu and Y. Yang, *ACS Nano*, 2014, **8**, 1674.
3 J. Burschka, N. Pellet, S.-J. Moon, R. Humphrey-Baker, P. Gao, M. K. Nazeeruddin and M. Grätzel, *Nature*, 2013, **499**, 316.
4 P. Docampo, F. Hanusch, S. D. Stranks, M. Döblinger, J. M. Feckl, M. Ehrensperger, N. K. Minar, M. B. Johnston, H. J. Snaith and T. Bein, *Adv. Energy Mater.*, 2014, **4**, 1400355.
5 A. Kojima, K. Teshima, Y. Shirai and T. Miyasaka, *J. Am. Chem. Soc.*, 2009, **131**, 6050.
6 J. H. Im, C. R. Lee, J. W. Lee, S. W. Park and N. G. Park, *Nanoscale*, 2011, **3**, 4088.
7 H.-S. Kim, C.-R. Lee, J.-K. Im, K.-B. Lee, T. Moehl, A. Marchioro, S.-J. Moon, R. Humphry-Baker, J.-H. Yum, J. E. Moser, M. Grätzel and N.-G. Park, *Sci. Rep.*, 2012, **2**, 591.
8 M. M. Lee, J. Teuscher, T. Miyasaka, T. N. Murakami and H. J. Snaith, *Science*, 2012, **338**, 643.
9 J. M. Ball, M. M. Lee, A. Hey and H. J. Snaith, *Energy Environ. Sci.*, 2013, **6**, 1739.
10 D. Bi, S.-J. Moon, L. Haggman, G. Boschloo, L. Yang, E. M. J. Johansson, M. K. Nazeeruddin, M. Grätzel and A. Hagfeldt, *RSC Adv.*, 2013, **3**, 18762.
11 H.-S. Kim, I. Mora-Sero, V. Gonzalez-Pedro, F. Fabregat-Santiago, E. J. Juarez-Perez, N.-G. Park and J. Bisquert, *Nat. Commun.*, 2013, **4**, 2242.
12 M. Liu, M. B. Johnston and H. J. Snaith, *Nature*, 2013, **501**, 395.
13 E. Edri, S. Kirmayer, A. Henning, S. Mukhopadhyay, K. Gartsman, Y. Rosenwaks, G. Hodes and D. Cahen, *Nano Lett.*, 2014, **14**, 1000.
14 J. J. Choi, X. Yang, Z. M. Norman, S. J. I. Bilinge and J. S. Owen, *Nano Lett.*, 2014, **14**, 127.
15 K. K. Bass, R. E. McAnally, S. Zhou, P. Djurovich, M. E. Thompson and B. Melot, *Chem. Commun.*, 2014, **50**, 15819.
16 T. Ripolles-Sanchis, A. Guerrero, J. Bisquert and G. Garcia-Belmonte, *J. Phys. Chem. C*, 2012, **116**, 16933.
17 A. Abrusci, S. D. Stranks, P. Docampo, H.-L. Yip, A. K.-Y. Jen and H. J. Snaith, *Nano Lett.*, 2013, **13**, 3124.
18 H. Zhou, Q. Chen, G. Li, S. Luo, T.-B. Song, H.-S. Duan, Z. Hong, J. You, Y. Liu, T. Liu and Y. Yang, *Science*, 2014, **345**, 542.
19 L. Brus, *J. Phys. Chem.*, 1986, **90**, 2555.
20 G. Giorgi, J.-I. Fujisawa, H. Segawa and K. Yamashita, *J. Phys. Chem. Lett.*, 2013, **4**, 4213.
21 R. Lindblad, D. Bi, B.-W. Park, J. Oscarsson, M. Gorgoi, H. Siegbahn, M. Odelius, E. M. J. Johansson and H. Rensmo, *J. Phys. Chem. Lett.*, 2014, **5**, 648.
22 J. Evan, L. Pedesseau, J.-M. Jancu and C. Katan, *J. Phys. Chem. Lett.*, 2013, **4**, 2999.
23 L. Chai, R. T. White, M. T. Greiner and Z. H. Lu, *Phys. Rev. B: Condens. Matter Mater. Phys.*, 2014, **89**, 035202.
24 H. G. Agrell, G. Boschloo and A. Hagfeldt, *J. Phys. Chem. B*, 2004, **108**, 12388.
25 J. H. Heo, S. H. Im, J. H. Noh, T. N. Mandal, C.-S. Lim, J. A. Chang, Y. H. Lee, H.-J. Kim, A. Sarkar, Md. K. Nazeeruddin, M. Grätzel and S. I. Seok, *Nat. Photonics*, 2014, **7**, 486.

